Liquidlike Spatial Distribution of Magnetic Droplets Revealed by Neutron Scattering in $La_{1-x}Ca_xMnO_3$

M. Hennion,[1] F. Moussa,[1] G. Biotteau,[1] J. Rodríguez-Carvajal,[1] L. Pinsard,[2] and A. Revcolevschi[2]
[1]*Laboratoire Léon Brillouin, CEA-CNRS, CE Saclay, 91191 Gif sur Yvette Cedex, France*
[2]*Laboratoire de Chimie des Solides, Université Paris-Sud, 91405 Orsay Cedex, France*
(Received 29 December 1997; revised manuscript received 27 May 1998)

Elastic neutron scattering experiments, performed in semiconducting $La_{1-x}Ca_xMnO_3$ single crystals ($x = 0.05, 0.08$), reveal new features in the problem of electronic phase separation and metal insulator transition. Below T_N, the observation of a broad magnetic modulation in the q-dependent elastic scattering intensity, centered at nearly identical q_m whatever the q direction, can be explained by a liquidlike spatial distribution of similar magnetic droplets. A semiquantitative description of their magnetic state, diameter, and average distance can be done. Such a picture can explain the anomalous characteristics of the spin wave branches previously observed. [S0031-9007(98)06987-7]

PACS numbers: 75.50.–y, 61.12.Ex, 71.30.+h

Doped Mn perovskites are intensively studied for their remarkable giant magnetoresistance underlying the electronic behavior that has potential technological applications. The basic physical ideas have been given by Zener [1], with the model of the double exchange, which connects the electron hopping with the ferromagnetic (F) alignments of Mn spins. The electron-phonon coupling through the Jahn-Teller effect was studied by Millis *et al.* [2]. On the other hand, the rôle of the electronic localization and the formation of magnetic polarons has been emphasized by Varma *et al.* [3]. Several pictures of magnetic polarons were proposed, associated to one carrier (small polarons) [4,5] or, in the case of larger carrier densities, to several carriers (large polarons) [6]. A cooperative state of magnetic droplets by self-trapping carriers was predicted by Nagaev using the s-d or s-f model [6], since this physical situation was first suggested for some rare-earth compounds [7]. Models of the electronic phase diagram have recently been reexamined [8,9]. Magnetic inhomogeneities have been suggested to be the origin of the behavior of the susceptibility and of the dynamical spin fluctuations observed above T_c in doped Mn perovskites [10,11]. Very recent NMR experiments have been interpreted in terms of electronic phase separation [12]. However, a characterization of magnetic inhomogeneities has never been made until now. We have started a spin dynamics study in $La_{1-x}Ca_xMnO_3$ for low doping [13,14] where the system is insulating and undergoes a transition to a weakly canted antiferromagnetic (AF) state at T_N [15]. An additional spin wave branch occurs by doping. The corresponding dynamical susceptibility reveals a small ferromagnetic correlation length, whereas the dispersion curve is isotropic, indicating a new ferromagnetic coupling between some Mn spins. This isotropy contrasts with the strongly anisotropic character of the other spin wave branch, characteristic of super-exchange. This new spin dynamics was attributed to "magnetic polarons," whose origin could not be elucidated.

We have performed *elastic* neutron scattering measurements as a function of temperature in $La_{1-x}Ca_xMnO_3$ ($x = 0.05, 0.08$), close to the direct beam ($\tau = 0$) and the $\tau = (110)$ Bragg peak. In both experimental cases, a broad modulation is observed, centered at nearly the same q_m whatever the q direction, with intensity growing below T_N. This scattering does not exist for $x = 0$. Such a pattern is typical of an assembly of magnetic clusters or droplets, with a mean magnetization different from that of the matrix and a well-defined shortest distance between them. A semiquantitative description of the droplets and of their spatial distribution is proposed using a liquidlike model. The droplets are isotropic, their radius is ≈ 9 Å, their density is low compared to that of the hole concentration, and their minimal distance of approach indicates a repulsive interaction. The existence of these magnetic clusters is closely linked with the unusual spin dynamics [14,16,17]. The overall static and dynamic observations suggest a picture of magnetic droplets or large polarons with a magnetic coupling distinct from exchange, coupled through the surrounding medium characterized by the superexchange coupling. They are characteristic of an electronic phase segregation, which results from the balance between unmixing forces, predicted by the s-d model, and intermixing Coulomb forces.

Experiments have been carried out at the reactor Orphée (Laboratoire Léon Brillouin) using a triple axis spectrometer set at a cold neutron source. The samples with $x = 0.05$ and 0.08 show similar results, so that only observations for the $x = 0.08$ sample, with a volume of 0.3 cm^3, are reported. The crystalline structure is orthorhombic (O') with *Pbnm* symmetry. The crystals are twinned basically having three F domains of volume V_i ($i = 1, 2, 3$) with their c axes along the directions $\mathbf{a}_0$, $\mathbf{b}_0$, $\mathbf{c}_0$ of the cubic perovskite substructure [14]. The other type of domains where $\mathbf{a}$ and $\mathbf{b}$ are interchanged, leading to two peaks in the rocking curve, may have some influence only close to $\tau \neq 0$. The $\mathbf{q}$ directions [110], [001], [112], and [100] refers to $\mathbf{a}_0$, $\mathbf{c}_0$, to the diagonals

of the faces $(\mathbf{a}_0 + \mathbf{c}_0)$ and $(\mathbf{a}_0 + \mathbf{b}_0)$, respectively. The subscript i will be used below to distinguish the $\mathbf{q}$ direction within the different F domains. The magnetic structure mainly consists of ferromagnetic (**a**-**b**) planes, with AF stacking along **c**. However, the increase of the (110) and (112) nuclear Bragg peaks below T_N (122 K), indicates a long range ferromagnetic ordering for a small spin component along **c**. It corresponds to a canted state. At 14 K, the *average* canting angle, $\theta_{\rm av}$, is $\approx 10°$ from **b** within the (**b**-**c**) plane.

Elastic experiments have been performed around $\tau = 0$ with $k_i = 1.25$ Å^{-1}, covering six temperatures within the $15 < T < 300$ K and $0.05 < q < 0.6$ Å^{-1} ranges, along several $\mathbf{q}$ directions. Intensities have been put on an absolute scale, using a vanadium sample and a standard procedure for correction. The temperature dependence of the spectra are reported in Fig. 1a for $q \parallel [110]_1$. In the $150 < T < 300$ K range, $I(q) = I(q)_{\rm HT}$ is found temperature independent. In the smallest q range, $I(q)_{\rm HT}$ is attributed to dislocations or large structural defects present in the sample. At larger q, the residual intensity is nearly twice as large as the nuclear and chemical incoherent scattering (marked by the arrow in Fig. 1a), indicating a contribution from disordered spins, static at the experimental time scale (0.5×10^{-11} s). Below T_N, $I(q)$ increases significantly in the whole q range, except close to $q \approx 0.01$ Å^{-1}, and shows a modulation centered at $q_m \approx 0.2$ Å^{-1} at 15 K. The temperature dependence of q_m cannot be detected in the 75–15 K range within our accuracy. Similar observations are obtained along $[112]_1$ (mixed with $[100]_3$), except for a small shift of q_m towards a smaller value and a small overall decrease of intensity. $I(q)$ along $[001]_1$ (mixed with $[110]_{2,3}$), is identical to $I(q)$ along $[110]_1$. The same observations are obtained using an XY detector device (SANS), at 15 K where the dynamical spin fluctuations can be neglected.

Figure 1b reports the magnetic contribution $I_m(q)$ obtained by substracting $I(q)_{\rm HT}$, for $q \parallel [110]_1$ and $q \parallel [112]_1$ at $T = 15$ K. The smallest q range corresponding to effects related to the dislocations, is not shown.

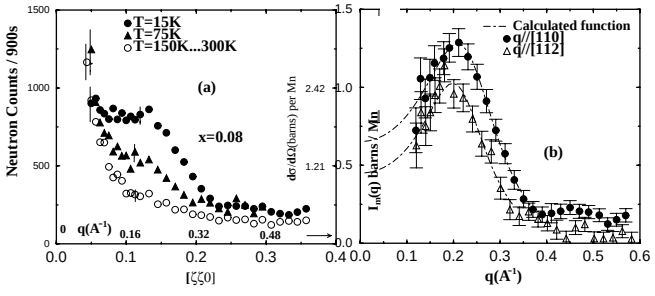

FIG. 1. (a) Scattering intensities versus q in counts and calibrated in barns, observed above $T_N = 122$ K $[I(q) = I(q)_{\rm HT}]$, at 75 and 15 K for $[110]_1$ direction. The arrow marks the nuclear incoherent scattering. (b) Magnetic intensities $I_m(q) = I(q) - I_{\rm HT}(q)$ versus q at 15 K for $[110]_1$, and $[112]_1$ directions. The dashed lines are calculated functions (c.f. the text).

$I_m(q)$ consists of a broad peak, located at $q_m \approx 0.21$ Å^{-1} and a residual and nearly flat scattering beyond 0.4 Å^{-1}. Along $[112]_1$, the overall intensity is slightly smaller, and a slight shift of q_m is observed.

Elastic experiments ($k_i = 1.55$ Å^{-1} with Be filter), have also been performed in the $([110],[001])$ plane close to $\tau = (110)_1$, at eight temperatures in the $11 < T < 300$ K range, and several $\mathbf{q}$ directions. The $[110]_1$ q direction is reported in Fig. 2a. In this figure, the two sets of vertical lines are results of the fit of the $(110)_1$ (bold) and $(002)_2$ Bragg peaks, easily resolved due to the large orthorhombicity. At 15 K, a well-defined maximum in $I(q)$ is observed at $\zeta = 0.87$ (i.d. $q_m = 0.2$ Å^{-1}), with a flat q scattering beyond 0.4 Å^{-1}). The q-symmetric intensity of this modulation with respect to $(110)_1$ is observed as a shoulder on the huge $(002)_2$ Bragg peak side of the twin domain, as shown in the inset of Fig. 2a.

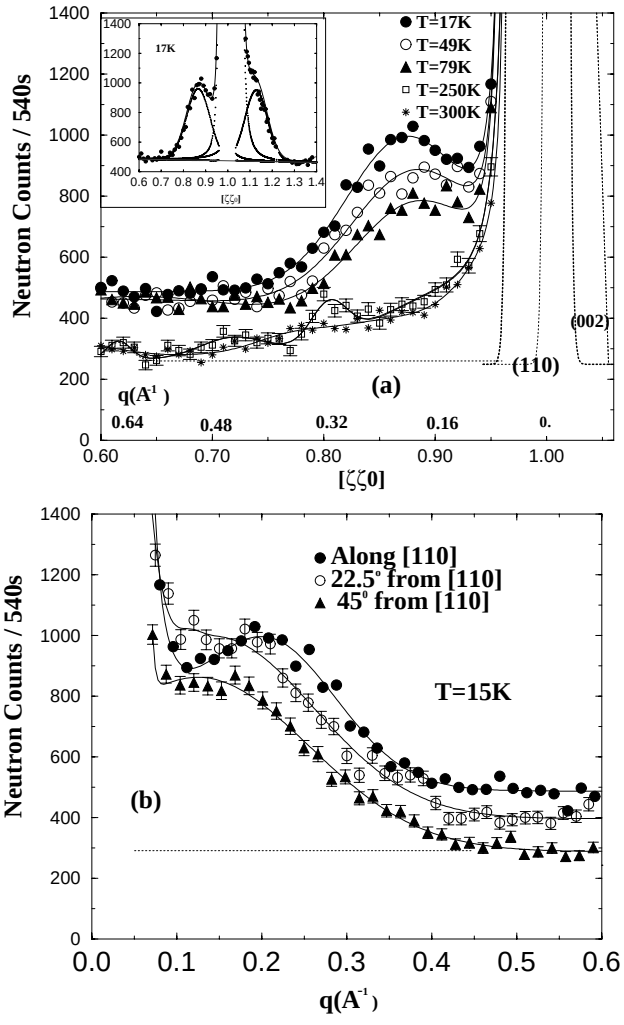

FIG. 2. Diffuse scattering intensities versus Q (or $q = Q - \tau$) measured around $\tau = (110)_1$. (a) along $[110]_1$, at five temperatures in the 300–17 K range ($T_N = 122$ K). When not shown, the error bar is within the size of the symbol. In the inset, the continuous lines are components of a fit with two $(+q_m, -q_m)$ modulations, symmetric with respect to $(110)_1$. (b) At 15 K along three q directions. The horizontal line locates the sample background observed at 300 K [cf Fig. 2(a)].

The apparent asymmetry of the spectrum is due to the superposition of $(002)_2$ and $(110)_1$ Bragg peaks with no modulation from the domain $(002)_2$. We conclude that this modulation is magnetic, with a magnetization along (001). In Fig. 2b, $I(q)$ is reported for **q** along two other directions of the scattering plane at 15 K, taking the *same* q origin at $(110)_1$. A small overall decrease of the intensity and a shift of q_m to smaller values is observed. Along $[112]_1$, the q_m value appears slightly smaller than that observed close to $\tau = 0$ (Fig. 1). This is well explained by the shift of the q origin attached to the different domains, unlike the previous case, close to $\tau = 0$, where the q origin is the *same* for all domains. The intensity is smaller by a nearly q independent value. Actually, the intensity of the flat q tail keeps the low value determined at 300 K [c.f. the horizontal lines in Figs. 2a and 2b], whereas along the other directions it varies with temperature. As the temperature increases, a very slight decrease of q_m can be detected, whereas the intensity of the modulation decreases (Fig. 2a). At T_N, a huge critical scattering intensity is observed close to the $(110)_1$ Bragg peak. In the $T_N < T < 250$ K range, small modulations appear, but along $[110]_1$ ($\mathbf{a}_0$ axis) only. As shown at 250 K in Fig. 2a, the q maxima correspond to the harmonics of q_m. Their intensities show irreversibilities with temperature, in contrast with the broad modulation below T_N which is perfectly reproducible. Since undetected close to $\tau = 0$, they are likely related to modulated strain effects (with a $Q = \tau + q$ dependent intensity) coexisting or competing with the broad magnetic modulation. At 300 K, $I(q)$ is monotonous, but its weak q dependence indicates the persistence of ferromagnetic correlations, static at the experimental time scale. These observations confirm those obtained close to the direct beam. The flat q scattering, with minima of intensity along [112], appears as a "sample background" corresponding to mainly disordered spins, the origin of which is unclear.

We focus our analysis on the magnetic contribution $I_m(q)$ obtained close to $\tau = 0$ at 15 K (Fig. 1b). A scattering pattern showing a broad modulation with nearly the same q_m in all **q** directions, indicates a spatial organization of similar entities or "droplets," as that observed, e.g., in a chemical unmixing process [18]. To apply this model in a magnetic system, one needs to define a mean magnetization density into the two regions, with a "contrast" between them, as an analog of the chemical contrast. The existence of a ferromagnetic component along **c** allows one to define a magnetization function $\mathbf{m}(\mathbf{r})$, $\mathbf{m} \parallel \mathbf{c}$ throughout the lattice. Therefore, the spatial Fourier transform of the spin correlations $\langle S_i S_j \rangle$ is replaced by that of $\langle \mathbf{m}(\mathbf{r})\mathbf{m}(\mathbf{r}') \rangle$, **r** being a continuous variable in direct space. Neglecting the small anisotropy, a semiquantitative analysis can be made using

$$d\sigma(q)/d\Omega = r_0^2 A N_V V_d^2 |\Delta m|^2 |F(qR)^2| J(q), \quad (1)$$

where Δm is the difference between the mean magnetizations $\mathbf{m} \parallel \mathbf{c}$ inside and outside the droplet. $F(qR)$ is the form factor of the droplet (a spherical shape of radius R is assumed) of density N_V and volume V_d and $J(q)$ is the interference function. The A factor ($A = \sum_i V_i \sin^2 \theta_i / \sum_i V_i$ where θ_i is the angle between the mean magnetization **m** and **q** for the domain V_i) is required to determine Δm. It expresses that for a **q** direction belonging to domain 1, the intensity also comprises contributions from domains 2 and 3. They have different **q** and **m** directions and are weighted by their geometrical factor $\sin^2 \theta_i$. This latter factor shows that [110] is a "pure" direction, [001] cannot be observed, and [112] is mixed with [100], weighted by $0.5(V_1 + V_2)$ and V_3, respectively. The equality of the three twinned volumes could be checked at 11 K from the scattering pattern of the SANS experiment, thanks to the XY detectors device. We have used the isotropic $J(q)$ function derived for liquids by Ashcroft and Lekner [19]. The spatial distribution is characterized by two parameters: the particle density N_V from which we determine the mean interparticle distance d_m and the minimal distance of approach between the particle centers $d_{\min}$. The expression of $J(q)$ is given in the footnote [20]. This model can fit the experimental data as shown in Fig. 1b (dashed line). It yields a diameter $2R \approx 17$ Å (i.e., $\approx 4-5$ lattice parameter a_0 of the small perovskite cube), a droplet density $N_V = 2.1 \times 10^{-5}$ Å^{-3} leading to $d_m \approx 9a_0$, and a minimal distance of approach $d_{\min} = 26$ Å ($6 \sim 7a_0$). This value, compared to the average distance d_m, accounts for the rather well-defined organization and indicates a repulsive interaction between the droplets. From the absolute value of the intensity, we determine a magnetic "contrast" $\Delta m \approx (0.7 \pm 0.20)\mu_B$. It corresponds to a difference of $\approx 10°$, between the canting angles characteristic of the two regions, which is surprisingly small.

From this semiquantitative determination, we conclude that the density of the "ferromagnetic" particles is very low compared to that of the holes (ratio $1/60$ for $x = 0.08$) leading to a picture of hole-rich droplets within a hole-poor medium [6,8,9]. At $x = 0.08$, the magnetic state of the droplet is far from a true ferromagnetic state within the canted antiferromagnetic medium. It appears canted, the spins inside the droplets being deviated from the perfect AF structure by an angle of $\approx 20°$ ($\theta_{\text{av}} \approx 10°$). The temperature variation of the intensity below T_N, must be related to the evolution of the contrast Δm between the two magnetic regions, which varies with the mean magnetization. The almost temperature independent evolution of q_m suggests that the charge carrier segregation persists at T_N. Above T_N, where the spatial distribution described above cannot be observed, the information arises from the spin dynamics only, which indicates a ferromagnetic correlation length typical of these inhomogeneities [16].

We compare now the characteristics of the static magnetic inhomogeneities with those of the low energy spin

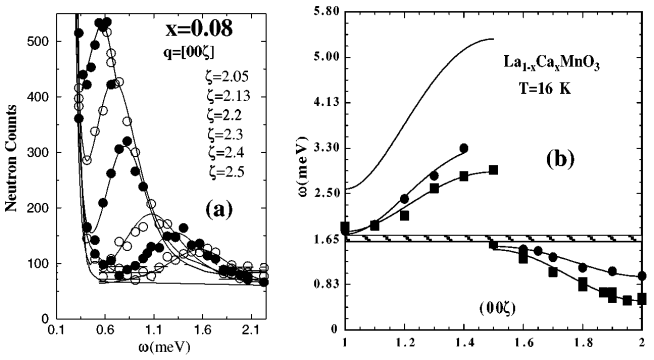

FIG. 3. (a) Energy scans fitted by energy Lorentzians for $q \parallel [00\zeta]$ at 16 K. From top to bottom, ζ varies from 2.05 to 2.5. (b) Dispersion curves for $x = 0.05$ (filled circle) and $x = 0.08$ (filled square). The continuous line at upper energy corresponds to the spin wave branch observed in pure $LaMnO_3$.

wave branch which appears for these doped systems, considering both its q-dependent intensity and its dispersion curve.

In Fig. 3a we have reported some energy spectra obtained as a function of $\mathbf{q} \parallel [001]$. Similar results are observed for $\mathbf{q} \parallel [110]$, indicating an isotropic and weakly dispersed spin wave branch. As previously shown for $x = 0.05$ [15], the intensity of this spin wave branch strongly decreases with q. Fitting the dynamical form factor (or energy integrated intensity) with a Lorentzian function leads one to determine a ferromagnetic correlation length ξ with $\xi \approx 7.5-8$ Å for both [110] and [001]. This reveals a tight connection between this low energy spin wave branch, characteristic of a low and isotropic coupling, with the static droplets described above. Among other characteristic features, these spin excitations keep a propagative character and are still well defined even at small q, i.e., over distances larger than the droplet size. These excitations may therefore correspond to eigenstates of the whole spin system. Within the above inhomogeneous picture derived from the static study, this means that the droplet magnetic states are coupled together through the matrix. In Fig. 3b, the dispersion curve is shown along [001] together with that of the other spin wave branch. The two spin wave branches observed for $x = 0.05$ are also reported for comparison. When considering the dispersion curve of the low-energy branch, a fit using $\omega = Dq^2 + \omega_0$ as an approximation at small q, indicates an increase of the stiffness constant D with x, and a decrease of the gap at $\tau = (002)$. Such an evolution of the constant D with the number of carriers can be expected at larger doping, within the true metallic and ferromagnetic state [21]. However, within the present picture of two magnetic regions, we observe a very peculiar evolution of the dispersion curves with x. The corresponding two spin wave branches keep separated by an energy gap, independent of x (hatched area in Fig. 3b). Such a peculiarity also holds at $x = 0.1$. Therefore, the separation in the direct space into two magnetic regions, induced by an electronic phase segregation is associated with a separation in the energy space into two spin dynamics, characteristic of two types of magnetic coupling.

In conclusion, the very unusual features found for the static and dynamical spin correlations provide new insights in the physics of the electronic phase separation. A liquidlike spatial distribution of magnetic polarons has been observed for the first time. The picture of hole-rich droplets agree with predictions of the s-d model in a well-known limit [6,8,9]. Whether such inhomogeneities exist at higher concentration, in the temperature range close to the metal-insulator transition where giant magnetoresistance properties are observed, is likely, but a confirmation requires more studies.

One author (M. H.) is very indebted to B. Hennion and D. Khomskii for fruitful discussions and G. Coddens for his critical reading of the manuscript.

[1] C. Zener, Phys. Rev. **82**, 403 (1951).
[2] A. J. Millis *et al.*, Phys. Rev. Lett. **77**, 175 (1996).
[3] C. M. Varma, Phys. Rev. B **54**, 7328 (1996).
[4] P. G. de Gennes, Phys. Rev. **118**, 141 (1960).
[5] T. Kasuya and A. Yanase, Rev. Mod. Phys. **40**, 684 (1968).
[6] E. L. Nagaev, Phys. Status Solidi B **186**, 9 (1994).
[7] N. Oliveira *et al.*, Phys. Rev. B **5**, 2634 (1972).
[8] S. Yunoki *et al.*, Phys. Rev. Lett. **80**, 845 (1998).
[9] M. Kagan, M. Mostovoy, and D. Khomskii (to be published).
[10] J. W. Lynn *et al.*, Phys. Rev. Lett. **76**, 4046 (1996).
[11] J. M. De Teresa *et al.*, Nature (London) **386**, 256 (1997).
[12] G. Allodi *et al.*, Phys. Rev. B **56**, 6036 (1997).
[13] F. Moussa *et al.*, Phys. Rev. B **54**, 15 149 (1996).
[14] M. Hennion *et al.*, Phys. Rev. B **56**, R497 (1997).
[15] E. O. Wollan and W. C. Koehler, Phys. Rev. **100**, 545 (1955).
[16] F. Moussa *et al.*, Physica (Amsterdam) **241B–243B**, 445 (1998).
[17] M. Hennion *et al.*, J. Magn. Magn. Mater. **177–181**, 858 (1998).
[18] M. Hennion *et al.*, Acta Metall. **30**, 599 (1982).
[19] N. W. Ashcroft and J. Lekner, Phys. Rev. **145**, 83 (1966).
[20] $J(q) = [1 - N_V B(q, N_V, d_{\min})]^{-1}$, with $B = -4\pi d_{\min}^3 \int ds s^2(\alpha + \beta s + \delta s^2) \sin(sqd_{\min})/sqd_{\min}$, and α, β, and δ related to $\eta = \pi N_V d_{\min}^3/6$ (c.f. [19]).
[21] K. Kubo and N. Ohata, J. Phys. Soc. Jpn. **33**, 21 (1972).